Collision-enhanced resonance of laser-diode-excited Cs in a buffer gas

F. de Tomasi, M. Allegrini, and E. Arimondo
Dipartimento di Fisica, Universitá di Pisa, Piazza Torricelli 2, I-56126, Pisa, Italy

G. S. Agarwal* and P. Ananthalakshmi
School of Physics, University of Hyderabad, Hyderabad-500134, India
(Received 29 December 1992)

We report an experimental investigation of the Cs D_2 line-shape changes due to laser-induced optical pumping and collisions in a buffer gas. A model dealing with the population of the ground-state hyperfine levels, the pressure broadening in the presence of Ne, and the diffusion of the atoms outside the laser beam describes well the complex line shapes.

PACS number(s): 32.80.Bx, 42.50.−p

I. INTRODUCTION

Three-level atomic systems present a rich variety of phenomena when excited by resonant or near-resonant radiation. Among the stationary phenomena, optical pumping, i.e., preparation of atoms in a well defined state, has been the subject of a large number of investigations. Thus it may be supposed that all the theoretical and experimental aspects of three-level spectroscopy would be well known. On the contrary, performing some very simple experiments of laser spectroscopy in the Doppler-broadened regime with a laser diode on a cell containing an alkali vapor, cesium, and buffer gas at low pressure, we observed a striking change in the behavior of the fluorescence signal as a function of the laser frequency. The maximum in the fluorescence signal did not appear when the laser was tuned to resonance with either of the two absorption lines associated to the hyperfine splitting in the ground state, but rather when the laser frequency was tuned to the center between the two hyperfine components, well outside the Doppler profile of each hyperfine component. This experimental observation finds its explanation in the hyperfine optical pumping into either of the two hyperfine ground-state levels: the maximum absorption, hence the maximum fluorescence, occurs when the hyperfine optical pumping into the two levels is equal. This competing effect of the hyperfine pumpings occurs for a pump laser tuned halfway between the two hyperfine components of the optical transition. As an alternative explanation, for a laser tuned into resonance with either of the two hyperfine transitions, hyperfine optical pumping into a state noncoupled with radiation takes place, and the absorption-fluorescence signal decreases. Such optical pumping will here be denoted as "dark state" optical pumping, while "bright state" optical pumping will be referred to a state always coupled with the radiation, producing maximum absorption and fluorescence. For an alkali atom with hyperfine splitting in the ground state, this bright optical pumping is achieved when the laser radiation produces equal excitation rates for the two ground hyperfine states. Its overall behavior depends on the efficiency of the hyperfine optical pumping, hence it may be observed very clearly in cells where the presence of buffer gas enhances the pumping.

An important result of our experimental observations on cesium vapor is that the maximum of the cesium optical pumping into the bright state is observed when the laser is detuned by 4 GHz off each hyperfine transition. Thus the fluorescence signal observed in a cesium cell containing buffer gas is originated by atoms absorbing very far in the wings of the absorption line shape. Comparing the Gaussian and Lorentzian line shapes, associated, respectively, with the Maxwell-Boltzmann velocity distribution and with the buffer gas collisional broadening, we derive that in the experimental conditions the Lorentzian collisional broadening is the main contribution for the absorbing atoms far in the line-shape wings. Thus the cesium atoms which contribute to fluorescence absorb laser radiation because, from the interaction with the buffer gas, they experience a modification in the energy separation of the atomic levels. This energy modification is ten times larger than the inhomogeneous broadening of the optical transition. The modification of atomic line shape by interaction with buffer gas, with a large energy shift of the atomic transition resulting from the interaction with buffer gas, has been well investigated in laser experiments using strong laser sources [1]. It is an interesting result of this experiment that using a laser source in the milliwatt range, it is possible to monitor these modifications.

Among the optical pumping experiments dealing with preparations of atoms into states either dark or bright, i.e., noncoupled or coupled with radiation, it may be noticed that the term "bright line" has been already introduced in the case of a three-level system in Λ configuration interacting with two laser fields exciting atoms from the ground state to the excited one [2], within the context of coherent population trapping [3]. It should be stressed that the two concepts, of "bright state" introduced here and that of "bright line" introduced previously, are quite different [4], even if in our opinion the bright line of coherent population trapping has not yet received a complete physical interpretation. That bright line is related

to the preparation of atoms in a coherent superposition of atomic wave functions, while the bright state of the present investigation is not necessarily associated with a coherent superposition, and in fact we present an interpretation of the phenomenon based on a rate-equation model.

The process of optical pumping into a bright state has already been studied in sodium atoms [5], for which large laser intensities have been available for a long time using dye lasers and optical pumping has been examined extensively. For other alkali atoms, experimental investigations of bright optical pumping have not been reported. However, the numerical simulations performed for the analysis of light-induced drift of sodium and rubidium in noble gases have clearly reproduced this phenomenon of optical pumping in a bright state [6]. Finally we are aware of modification in the saturation spectroscopy of sodium atoms reported in [7], that could be explained on the basis of the optical pumping mechanism here analyzed. The modification in the fluorescence spectrum associated with bright state optical pumping is less evident in the case of sodium atoms, where the distance between the two hyperfine components is comparable to the Doppler linewidth. Thus for sodium the bright state pumping does not appear on the fluorescence spectrum at laser frequencies completely different from those of the expected absorption lines.

The influence of buffer gas, and neon specifically, on the absorption and optical pumping processes of cesium atoms, has been well studied, although, to our knowledge, no investigation of optical pumping into the bright state has been reported so far. For what concerns the absorption profile, very broad emission bands have been observed from microwave discharge excited mixtures of cesium vapor and low-density noble gas [8], even at the low pressures of the present investigation. The presence of these absorption bands has no particular influence on the fluorescence spectra we report, except that it contributes to enhance the absorption probability for the off resonant excitation. For what concerns optical pumping, the addition of buffer gas is important for confining the alkali atoms within the region of interaction with the laser radiation and obtaining long interaction times with the radiation, before a depolarization process by collisions with the wall or with the buffer gas itself takes place [9]. Use will be made in our analysis of results derived in the optical pumping studies. In optical pumping with laser sources, small amounts of inert buffer gas produce velocity-changing collisions that allow a redistribution of the atomic velocities without reequilibrating the populations of the atomic levels. In this way velocity-changing collisions permit optical pumping of the entire Doppler distribution [10]. Velocity-changing collisions certainly play an important role in our experiment on the laser diode excitation of cesium atoms in the presence of low pressure buffer gas. The kernel for velocity-changing collisions in cesium has not been explicitly determined, but it may be supposed not very different from that recently determined on rubidium atoms in [11]. The velocity-changing collisions have not been precisely modeled in our theoretical analysis, but we have performed some modeling supposing that collisions with the buffer gas produce a complete reequilibration within the velocity distribution. One final point requiring a more precise modeling in our experiment is the occurrence of radiation trapping, that is not very severe in the experimental conditions, but still it could affect the rates of pumping into the atomic states, as shown in the rate-equation model involving the radiation trapping effect formulated in [12].

The present paper is organized with a presentation of the experimental apparatus in Sec. II, a detailed discussion of the experimental results in Sec. III. Section IV discusses the theoretical modeling. In the conclusions we analyze the validity and the deficiency of our model in interpreting the experimental results and compare our theoretical analysis to that of Ref. [5].

II. EXPERIMENT

Our experimental arrangement is shown in Fig. 1. A laser diode, model STC LT-50A, with output in the several tens of milliwatts, has been used to excite the D_2 resonance line of cesium. The diode laser was powered by a battery through a current regulation circuit, and its temperature stabilized to a 2 mK accuracy through a standard circuit [13]. The linewidth of the laser diode in this free-running regime is 10 MHz. Frequency tuning of the laser has been realized by scanning the injection current. For some fluorescence observations, narrowing of the laser diode linewidth down to better than 1 MHz has been realized through optical feedback from a grating [13]. A magneto-optical isolator, model IO-5-NIR by Optical Research, avoids optical feedback on the laser diode from the fluorescence cell and all the measuring equipment. A spectrum analyzer, model 240 by Coherent, with 1500 MHz free spectral range, has provided a continuous monitor of the laser frequency during the laser scanning. A wavemeter was employed to measure the laser frequency at the beginning and end of each laser scan. An auxiliary cesium cell was occasionally used to observe absorption Lamb dips which served as an absolute frequency reference.

The parallel laser beam, with transverse radius 1 mm, propagated through a cylindrical glass cell, 30 mm in diameter and 110 mm in length, containing pure cesium or cesium plus neon buffer gas at different pressures. The fluorescent light from a total length of 20 mm starting

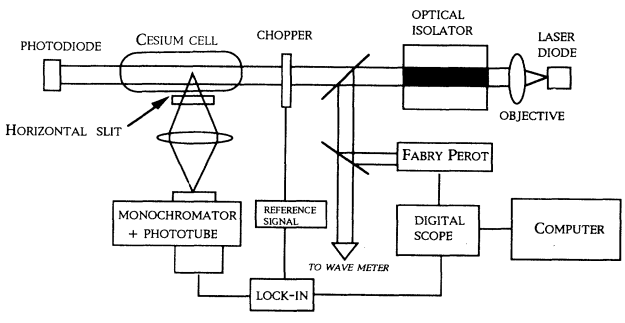

FIG. 1. Sketch of the experiment.

from the entrance window of the cell was focused, at right angles to the laser beam, on the horizontal entrance slit of a 1/3 m monochromator equipped with an extended S-20 photomultiplier. For some experimental observations a horizontal slit was located near the cell in order to limit the fluorescence collected from the cell to the region directly illuminated by the laser. In the spectra reported here the monochromator was not scanned but was tuned with slits wide open to the center of the D_2 cesium line, in order to collect all the fluorescence light emitted by the atoms. We checked that in our experimental conditions the fluorescence emission on the D_1 line, or from high lying levels, was negligible.

The light transmitted through the cesium cell was detected by a silicon photodiode that monitored the absorption of light by cesium atoms in the cell. The main aim of the cesium absorption detection at very low laser power, a few microwatts, was to test that within the experimental accuracy, five parts in a thousand, the cells filled with different buffer gas pressure contained the same cesium vapor pressure. The vapor density from standard tables is 1×10^{10} atoms/cm^3 at room temperature. From the measured small signal regime absorption, we have deduced that the 20 mm long detection region corresponded to a 0.4 absorption length. Thus the experiment was operated in conditions close to those where the radiation trapping phenomena could become important.

III. EXPERIMENTAL RESULTS

The cesium fluorescence emission was monitored at a given laser power, as a function of the laser diode frequency, for cesium cells containing no buffer gas and Ne buffer gas at 1, 5, and 50 Torr, respectively.

In the first part of the investigation the fluorescence light emitted by the cesium atoms near the entrance window of the glass cell was collected without spatial resolution in the direction transverse to the propagation one. The typical fluorescence observed in these conditions on the cell with pure cesium is reported in Fig. 2(a). Scanning the laser frequency, the excitation spectrum presents the two Doppler-broadened transitions starting from the F_g=3 and 4 hyperfine levels of the ground state to the hyperfine levels of the excited $2P_{3/2}$ state. The hyperfine structure of the excited state cannot be resolved in this Doppler-broadened spectrum, nor in those reported in the following. However, owing to the presence of the hyperfine structure and the optical pumping process between the ground-state levels, modifications in the shape of the Doppler-broadened fluorescence lines have been observed as a function of the laser power. For instance, the relative intensity of the total atomic fluorescence produced by the laser in resonance with the F_g=3 and 4 absorption lines depends on the laser power, and also on the laser frequency sweep rate, unless the sweep is very slow. We are not interested here in those line-shape modifications that we consider of minor scientific significance as compared to other ones.

When fluorescence detection without spatial resolution was performed on the cesium cell containing neon buffer gas, a strong modification of the fluorescence line shape was obtained. At low laser power the fluorescence spectrum contains the two ground-state hyperfine structure lines, but increasing the laser power the spectrum presents drastic deformations, with a large background. Finally at large laser power, around 100 mW/cm^2 for the 5 Torr cell, that background becomes a Lorentzian line shape centered between the two hyperfine components, as appears in the spectrum of Fig. 3.

The fluorescence signal in Fig. 3, detected without any spatial resolution, originates from an extended region of the cell around the laser beam core. As a consequence, the line shape is distorted because weak light in the spatial wings of the laser beam causes as much fluorescence as the strong light in the beam core. Thus we have modified the experimental detection geometry by inserting the slit near the cell, as described in the experimental setup, to restrict the detection region to the part illuminated directly by the laser beam core, at least in the vertical dimension. The insertion of this slit has also been effective in reducing the influence of radiation trapped light

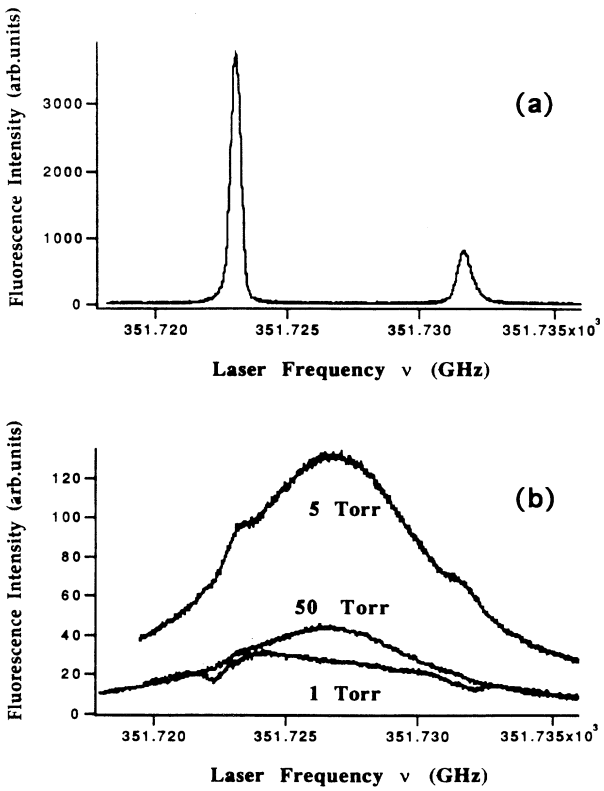

FIG. 2. Fluorescence signals vs laser frequency, observed in different cesium cells at laser intensity 400 mW/cm^2 with fluorescence detection spatially limited, through a horizontal slit, to 2 mm in the direction orthogonal to the laser propagation direction. (a) fluorescence observed on a cell at room temperature containing pure cesium vapor, (b) similar detection from cells containing Ne buffer gas at pressures 1, 5, and 50 Torr, respectively. In (a) and (b), the fluorescence intensity has been measured with the same arbitrary units for an easy quantitative comparison of the fluorescence signal as a function of the buffer gas pressure.

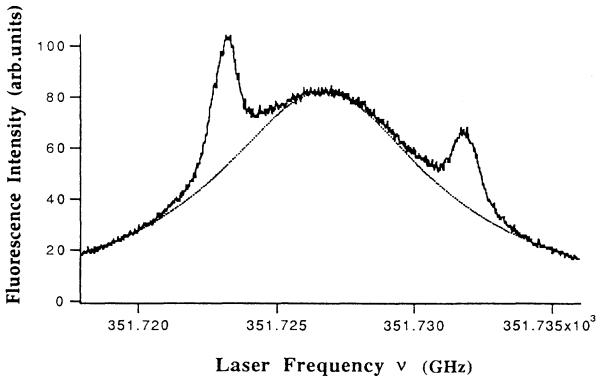

FIG. 3. Excitation spectra vs laser frequency for the 5 Torr neon cell at laser intensity 400 mW/cm^2, without spatial resolution in the detection collection. The two atomic hyperfine transitions are observed on top of a broad Lorentzian profile centered between the atomic lines. The dotted line represents a fit with a Lorentzian line shape centered at 371 726.8 GHz with full width at half maximum (FWHM) 9.5 GHz, about 0.4 GHz larger than the FWHM calculated from the density matrix approach.

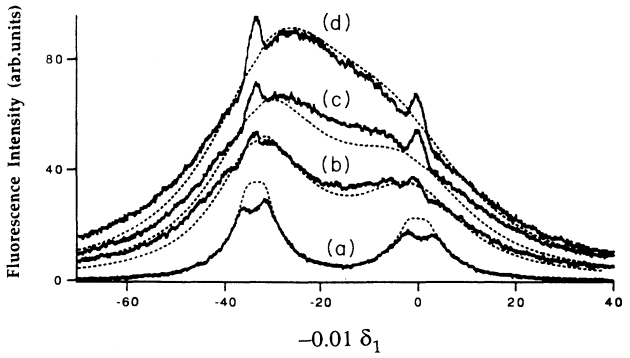

FIG. 4. Excitation spectra vs laser frequency for the 5 Torr neon cell at different laser powers, in the ratios 1:6.3:10:16 from (a) to (d). The laser intensity, estimated supposing the laser radiation is uniformly distributed over an area with 1 mm radius, is 120 mW/cm^2 in the case of curve (d), with a 20% uncertainty due to the radius measurement. On the horizontal axis the laser frequency detuning from the $F_g = 3$ atomic transition is reported in units of the spontaneous emission linewidth, $\delta_1 = \Delta_1/(A/2)$, for convenience of comparison with the theoretical curves. The dotted lines represent results of the numerical analysis based on the rate-equation model.

on the detected fluorescence spectrum. Moreover, in the final experimental setup we have used a laser propagation very close to the side walls since the self-absorption of fluorescence light in the horizontal propagation towards the monochromator entrance slit is reduced by a laser beam at grazing incidence near the side walls. In this configuration the hyperfine optical pumping could be affected by the cesium wall collisions, but we have not observed any modification on the excitation spectra for small displacements of the laser beam. Thus the fluorescence detection was limited to a region with nearly uniform laser intensity, without modification introduced by radiation trapping.

With this experimental arrangement, we have obtained the fluorescence spectra reported in Fig. 2(b), both for the cell without buffer gas and for the cells containing different pressures of buffer gas, at a fixed laser intensity, $I = 400$ mW/cm^2. The structures appearing in the spectra of Fig. 3, and corresponding to the Doppler-broadened hyperfine absorption lines, are eliminated in the spectra of Fig. 2(b), demonstrating that they are associated with phenomena taking place outside the region illuminated by the laser beam core. The spectra of Fig. 2(b) provide a clear evidence of the atomic preparation in an optically pumped bright state, with an efficiency depending on the buffer gas pressure, and passing through a maximum in the 5 Torr range. The experimental results for the broad structure are well fitted by a Lorentzian line shape centered between the two hyperfine absorption lines, having a width close to the hyperfine splitting in the ground state, as for the dotted line of Fig. 3.

Figure 4 reports experimental results for the fluorescence intensity versus laser frequency, at a fixed neon pressure, 5 Torr, and different laser intensities. The arrangement for spatial filtering is not as good as in Fig. 2(b), and the atomic transitions at the hyperfine frequencies have an intensity that, compared to that of the central resonance, is slightly larger than in the records of Fig. 2(b). The experimental results of Fig. 4 have been fitted through the model presented in the next section.

In Fig. 5 we show, as a function of the exciting laser intensity, the fluorescence intensity measured with the exciting laser frequency at the central position between the

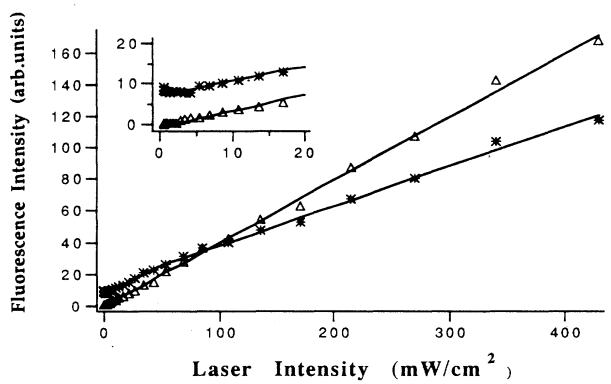

FIG. 5. Fluorescence intensity measured at the laser frequency centered between the F_g=3 and 4 hyperfine components (△) and at the laser frequency resonant with the F_g=3 optical transition (∗), versus the laser intensity. The straight line through the experimental points for the fluorescence intensity at the center, is in agreement with the predictions of the theoretical analysis. For the data concerning the F_g=3 atomic resonance, the best fit through the data was obtained by using two different straight lines at low and large laser intensities. The theoretical model cannot explain this behavior, but in the high intensity region the assumption of Maxwellian distribution of the atomic velocities may be questioned.

two hyperfine components and that measured at the maximum of the optical transition starting from the F_g=3 hyperfine ground state. The fit through the experimental data of the central fluorescence shows the linear dependence of this quantity on the laser intensity. We have verified that for intermediate values of the laser intensity, the ratio between the central fluorescence and the F_g=3 atomic fluorescence saturates towards a value that depends on the spatial filtering.

IV. THEORETICAL MODEL

The density matrix of the present system involves too many magnetic sublevels associated with $6S_{1/2}$ and $6P_{3/2}$ hyperfine components to allow its full evaluation. In order to understand the main features of the experimental results through the density matrix approach, we are forced to introduce some simplifications in the model. However, this simplified density matrix model predicts the main features of the experiment. The laser excitation to different hyperfine levels in the cesium excited state leads to different processes. Excitation to the recycling transitions F_g=3 $\longleftrightarrow$ F_e=2 and F_g=4 $\longleftrightarrow$ F_e=5 contributes to Zeeman optical pumping, but not to the hyperfine one. The first transition has a small probability, so that it is not relevant to the atomic evolution. For the linear polarization used in the present investigation, the Zeeman optical pumping on F_g=4 $\longleftrightarrow$ F_e=5 is not an efficient process. The two remaining excited hyperfine levels F_e=3 and 4 are coupled through the laser excitation to both hyperfine levels. For the experimental observations reported in this work, the coupling of the excited state to both ground hyperfine levels plays the key role. Thus in our simplified three-level model of cesium atoms analyzed by the density matrix approach, we will neglect the presence of the recycling transitions and will describe the excited hyperfine states as a single one, labeled as $|3\rangle$, see Fig. 6. Furthermore the pump field interacts on both the transitions $|1\rangle \longleftrightarrow |3\rangle$ and $|2\rangle \longleftrightarrow |3\rangle$ from the ground hyperfine states $|1\rangle$ and $|2\rangle$. The effects of collisions with the buffer gas are included in the model through the decay parameters Γ_{13} and Γ_{23} for the off-diagonal elements ρ_{13} and ρ_{23} of the density matrix. These decay rates are proportional to the pressure p of the buffer gas.

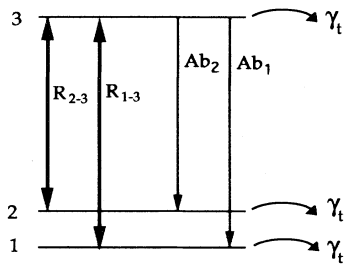

FIG. 6. Schematic representation of the three levels used in the theoretical model. The level $|1\rangle$ represents the $6\,^2S_{1/2}F_g$=3 ground state; the level $|2\rangle$ represents the $6\,^2S_{1/2}F_g$=4 one. The level $|3\rangle$ represents the $6\,^2P_{3/2}$ hyperfine levels coupled by optical transitions to both ground states. Spontaneous emission rates Ab_1, Ab_2, excitation rates $R_{i-3}, i = (1,2)$, and transit rate γ_t are indicated.

The complete density matrix equations for the three-level model system can be written as [14]

$$\begin{aligned}
\dot{\rho}_{33}(t) &= -A\rho_{33} - i\frac{\Omega_2}{2}(\rho_{32}-\rho_{23}) - i\frac{\Omega_1}{2}(\rho_{31}-\rho_{13}) \\
&\quad -\gamma_t\rho_{33}, \\
\dot{\rho}_{22}(t) &= Ab_2\rho_{33} + i\frac{\Omega_2}{2}(\rho_{32}-\rho_{23}) - \gamma_t(\rho_{22}-\rho_{22}^0), \\
\dot{\rho}_{11}(t) &= Ab_1\rho_{33} + i\frac{\Omega_1}{2}(\rho_{31}-\rho_{13}) - \gamma_t\left(\rho_{11}-\rho_{11}^0\right), \\
\dot{\rho}_{31}(t) &= -\left(\Gamma_{31} + \frac{A}{2} + \gamma_t + i\Delta_1\right)\rho_{31} \\
&\quad + i\frac{\Omega_1}{2}(\rho_{11}-\rho_{33}) + i\frac{\Omega_2}{2}\rho_{21}, \\
\dot{\rho}_{32}(t) &= -\left(\Gamma_{32} + \frac{A}{2} + \gamma_t + i\Delta_2\right)\rho_{32} \\
&\quad + i\frac{\Omega_2}{2}(\rho_{22}-\rho_{33}) + i\frac{\Omega_1}{2}\rho_{12}, \\
\dot{\rho}_{21}(t) &= -[i(\Delta_1-\Delta_2)+\gamma_t]\rho_{21} + i\frac{\Omega_2}{2}\rho_{31} - i\frac{\Omega_1}{2}\rho_{23}.
\end{aligned} \tag{1}$$

Here A^{-1} is the excited-state spontaneous emission lifetime, b_1 and b_2 are the branching ratios, assumed proportional to the statistical weights of the lower levels, γ_t^{-1} is the transit time, $\Delta_1 = \omega_{31} - \omega_l$ and $\Delta_2 = \omega_{32} - \omega_l$ are the frequency detunings of the laser frequency ω_l from the atomic transitions, and Ω_1 and Ω_2 are the Rabi frequencies of the field on the two atomic transitions. ρ_{11}^0 and ρ_{22}^0 denote the equilibrium populations of the levels in the absence of the field. Thus we have neglected the equilibrium population in the excited state. The equilibrium values of the populations in the ground states are supposed to be proportional to their statistical weights, i.e., $\rho_{11}^0/\rho_{22}^0 = b_1/b_2$, even if the three-level description introduced by Eqs. (1) represents a rough approximation, so that the exact magnetic degeneracies, with levels not interacting with the laser radiation, cannot be properly described. The motion of atoms is accounted for by replacing ω_l by $\omega_l - kv$ to derive the v-dependent density matrix $\rho(v)$. The quantity of interest for comparison with the experimental observations is

$$I = \lim_{t\to\infty}\langle\rho_{33}(v)\rangle, \tag{2}$$

where the angular bracket denotes the averaging with respect to the velocity distribution. We will deal with collisions rapidly thermalizing the velocity distribution

against the modifications due to the absorption/emission cycles. Thus, even in the presence of laser absorption, we assume that the Doppler velocity distribution is maintained:

$$P(v) = \frac{2k\sqrt{\ln 2}}{D\sqrt{\pi}} \exp\left[-4\ln 2\left(\frac{kv}{D}\right)^2\right], \tag{3}$$

with D the half-width frequency at half maximum.

A complete understanding of the solution of Eqs. (1) can be obtained only from the numerical work. However, there are special cases when the analytical solution can be obtained in closed form and it helps us in understanding what goes on in the experiment. For long transit times $\gamma_t^{-1} \to 0$, $\Omega_1 = \Omega_2 = \Omega$, $b_1 = b_2$ the steady-state solution of (1) leads to the following expression for the excited-state population:

$$\rho_{33} = \frac{\tilde{\Gamma}_{31}\tilde{\Gamma}_{32}\Omega^2\omega_{21}^2}{\mathcal{D}}, \tag{4}$$

$$\mathcal{D} = A\tilde{\Gamma}_{32}\left[(\Delta_1^2 + \tilde{\Gamma}_{31}^2)\omega_{21}^2 + \Omega^2\left(\frac{\Omega^2}{4} - \Delta_1\omega_{21}\right)\right] + \tilde{\Gamma}_{31}\left[(\Delta_2^2 + \tilde{\Gamma}_{32}^2)\omega_{21}^2 + \Omega^2\left(\frac{\Omega^2}{4} + \Delta_2\omega_{21}\right)\right] + 3\frac{\tilde{\Gamma}_{31}\tilde{\Gamma}_{32}\Omega^2\omega_{21}^2}{A}, \tag{5}$$

where we have introduced the energy separation ω_{21} between the two hyperfine components in the ground state and $\tilde{\Gamma}_{31} = \Gamma_{31} + A/2$, $\tilde{\Gamma}_{32} = \Gamma_{32} + A/2$. In Eq. (4) and in the following expressions for ρ_{33}, the v dependence was dropped since all the elements of the density matrix are proportional to $P(v)$. When desired, the v dependence is restored replacing ω_l by $\omega_l - kv$ and multiplying the density matrix elements by $P(v)$.

Let us now examine the features of the fluorescence as obtained on the basis of Eq. (4). For simplicity we set $\tilde{\Gamma} = \tilde{\Gamma}_{31} = \tilde{\Gamma}_{32} = \Gamma + A/2$; then Eq. (4) can be written in simplified form as

$$\rho_{33} = \frac{\tilde{\Gamma}A\frac{\Omega^2}{2}\omega_{21}^2}{\left(x - \frac{1}{2}\right)^2 + \frac{1}{4} + \frac{1}{4}\left(\frac{\Omega}{\omega_{21}}\right)^4 + \left(\frac{\tilde{\Gamma}}{\omega_{21}}\right)^2 + \frac{1}{2}\left(\frac{\Omega}{\omega_{21}}\right)^2\left(\frac{3\tilde{\Gamma}}{A} - 1\right)}, \tag{6}$$

where

$$x = \frac{\Delta_1}{\omega_{21}}. \tag{7}$$

Thus the fluorescence will have a resonance at $x = 1/2$ with half width $[\frac{1}{4} + \frac{1}{4}(\Omega/\omega_{21})^4 + (\tilde{\Gamma}/\omega_{21})^2 + \frac{1}{2}(\Omega/\omega_{21})^2(3\tilde{\Gamma}/A - 1)]^{1/2}$. This width does depend on the intensity of the pump I_L $(\propto \Omega^2)$, and on the pressure p through the dependence of the rate Γ. However, for the case of Cs D_2 transition and for pressures and Rabi frequencies used in the experiment $\Omega/\omega_{21} \ll 1$, $\Gamma \ll \omega_{21}$, and hence (4) reduces to a rather simple form

$$\rho_{33} = \frac{\frac{\Omega^2}{4\omega_{21}^2}\left(1 + 2\frac{\tilde{\Gamma}}{A}\right)}{\left(x - \frac{1}{2}\right)^2 + \frac{1}{4}}. \tag{8}$$

Thus the peak intensity depends on the laser intensity and on pressure in a simple way though we are dealing with a system where the optical transitions are saturated:

$$\rho_{33} \propto I_L, \tag{9}$$

$$\rho_{33} \propto \left(1 + \frac{2\Gamma_0 p}{A}\right), \tag{10}$$

where we have introduced $\Gamma = \Gamma_0 p$. The result (8) cannot be obtained from second-order perturbation theory although ρ_{33} appears to be proportional to the intensity of the pump, as reported in the experimental results of Fig. 5. It may also be noted that although at low pressures p the detected signal (4) increases monotonically with pressure, there is the possibility that for large collisional widths, comparable to ω_{21}, the signal would decrease. This follows from Eq. (6) for the peak height, that for large pressure varies as $\Gamma_0 p/(1 + \alpha p + \beta p^2)$, with α and β appropriate parameters. From this expression we derive that the peak height exhibits a maximum when $p = 1/\sqrt{\beta}$. This behavior is in agreement with the experimental results presented in Fig. 2(b) for the dependence of the fluorescence on the buffer gas pressure. However, the theory predicts that the maximum is reached when the collisional width is comparable to ω_{21} while in the experiment the maximum occurs at smaller collisional widths.

Thus we conclude that the fluorescence will exhibit resonance whenever the pump laser is tuned halfway between the two ground hyperfine levels. The width of this resonance is large and in fact is of the order of $\omega_{21}/2$. Note that the separation $\omega_{21}/2\pi$ (9192.63 MHz) is much larger than the Doppler width $2D/2\pi$ (375 MHz) and thus this resonance will be practically unaffected by Doppler averaging. In principle this resonance should be seen even in the absence of collisions. However, in practice the transit time is not infinite and this results in the appearance of the peaks in fluorescence at $\Delta_1 = 0$ and $\Delta_1 = \omega_{21}$ which are such that the peak at $\Delta_1 = \omega_{21}/2$ is not resolved. The collisions enhance [Eq. (10)] the peak at $\omega_{21}/2$. Figure 7 shows this behavior. For no collisions and $\gamma_t = 0$ (bottom curve), one has the broad resonance at $\Delta_1 = \omega_{21}/2$ which is lost, however, when we include the effects of finite transit time, $\gamma_t = 3.6 \times 10^{-3} A/2$ for the cesium atoms through the laser beam for neon pressure $p = 0$. For buffer gas pressures greater than approximately p =0.5 Torr (the exact value depending on the intensity of the pump), the resonance at $\omega_{21}/2$ starts becoming resolved and becomes rather prominent at much larger pressures. It is to be noticed that the peak at $\Delta_1 = \omega_{21}/2$ is relatively broad and thus is expected to be rather unaffected by Doppler broadening. In each

case corresponding to Fig. 7 we have checked that the Doppler averaging essentially does not affect the result or the excited-state population.

For the numerical calculations, all spectroscopic and collisional cesium parameters required for that comparison have been taken from standard references. For the transit relaxation rate γ_t we have used the standard results:

$$\gamma_t = \frac{2.405^2 D_g}{R^2}\left(\frac{1}{1+K/p}\right), \tag{11}$$

where 2.405 is the lowest zero of the zeroth-order Bessel function, R is the radius of the laser beam, $D_g = 98.6/p$ $\mathrm{cm^2\,sec^{-1}\,Torr^{-1}}$ is the diffusion coefficient of ground-state cesium atoms in the neon buffer gas, inversely proportional to the neon pressure, and K is the Knudsen coefficient defined as

$$K = c\frac{\bar{l}_p}{R}. \tag{12}$$

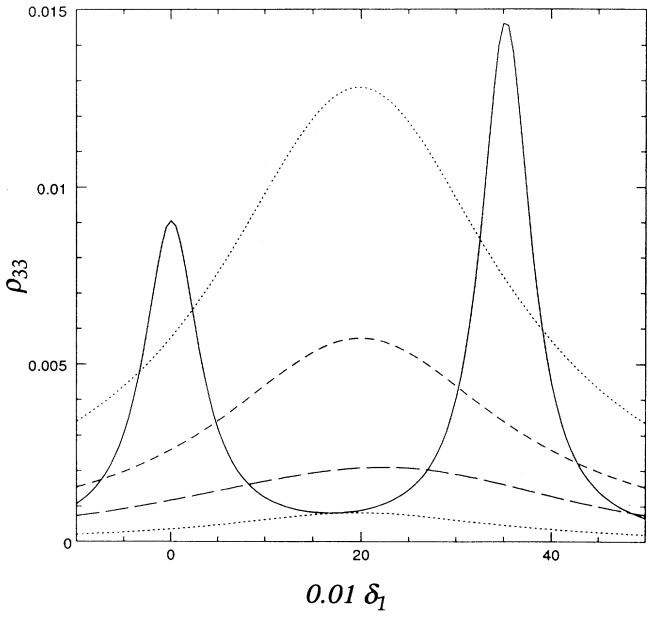

FIG. 7. Dependence of the excited-state occupation ρ_{33} on the laser frequency as obtained from the numerical analysis of Eq. (4). The laser frequency relative detuning $\delta_1 = \Delta_1/(A/2)$ has been reported on the horizontal axis. The Rabi frequencies $\Omega_1 = \Omega_2$ are fixed to $50A$, while different conditions of transit time and buffer gas pressure are explored. In the bottom curve for $p = \gamma_t = 0$ the broad line at $\Delta_1 = \omega_{12}/2$ is obtained. The results for the excited-state occupation in the presence of transit time damping rate are represented by the solid line, corresponding to $\gamma_t = 3.6 \times 10^{-3} A/2$ and $p = 0$. It may be noticed that the atomic transitions are recovered in the spectrum. Increasing the buffer gas pressure, the broad structure is reobtained in the excited-state occupation; the dashed curves correspond to different values of buffer gas pressure: from bottom to top $p = 0.5$ Torr, $p = 2.0$ Torr, $p = 5.0$ Torr, respectively, with corresponding γ_t derived from Eq. (11). All the results are not modified by the Doppler averaging.

Here $\bar{l}_p = 5.5310^{-3}/p$ cm/Torr is the mean free path and c is a numerical constant equal to 6.8 for a hard-sphere interaction [9]. For low neon gas pressure the transit rate reduces to the reciprocal time of flight of a cesium atom through the laser beam. For large neon gas pressure the transit rate is determined by the diffusion rate through the laser beam dimension. The decay parameters Γ_{31} and Γ_{32} are determined by the cesium-neon pressure broadening coefficients of Ref. [15]: $\Gamma_{31} = \Gamma_{32} = 8.0 \times 10^7 p$ $\mathrm{sec^{-1}}$ Torr. The velocity-changing collisions also lead to rapid decay of the optical coherences, that could be included in Eqs. (1) through proper values of Γ_{31} and Γ_{32}. However, we are not aware of any specific study of velocity-changing collisions in cesium vapors.

Figure 8 shows the effect of both changing the intensity of the pump and the pressure. It is seen that at moderate pressures the structure at $\omega_{21}/2$ is not resolved if the pump intensity is low. Now in Fig. 8 we have incorporated the fact that the branching ratios b_1 and b_2 are unequal. Taking into account that the two-level saturation intensity of the cesium resonance for homogeneous broadening is 2.20 $\mathrm{mW/cm^2}$, it turns out that the Rabi frequencies introduced in Figs. 7 and 8 are of the same order of magnitude as those applied in the experimental investigations.

While the above analysis yields broadly the experimental feature, it cannot predict correct quantitative results, as one has to account for the magnetic degeneracies of the levels including the actual number of hyperfine components taking part in optical transitions. In principle the analysis could be generalized but then it becomes extremely complex as one has to deal with the density matrix of a system with a large number of levels. Thus we have looked into the predictions of a simple rate-equation model where we can incorporate the effects of degeneracies and statistical weights easily. As before, this model will be based on the hypothesis of very efficient velocity-changing processes, so that the Maxwellian distribution of velocities, given by Eq. (3), is preserved even in presence of laser absorption. Thus the rate equations for the populations n_i in states $i = 1, 3$, integrated over the velocity distribution, can be written in the form

$$\begin{aligned}
\dot{n}_1 &= R_{1-3}\left(\frac{g_1}{g_3}n_3 - n_1\right) + b_1 A n_3 + \gamma_t\left(\frac{g_1}{g_1+g_2} - n_1\right),\\
\dot{n}_2 &= R_{2-3}\left(\frac{g_2}{g_3}n_3 - n_2\right) + b_2 A n_3 + \gamma_t\left(\frac{g_2}{g_1+g_2} - n_2\right),\\
\dot{n}_3 &= -R_{1-3}\left(\frac{g_1}{g_3}n_3 - n_1\right) - R_{2-3}\left(\frac{g_2}{g_3}n_3 - n_2\right)\\
&\quad -An_3 - \gamma_t n_3,
\end{aligned} \tag{13}$$

where g_i gives the degeneracy factor for state i, and where, as for the density matrix Eqs. (1), we have supposed that the γ_t damping mechanism produces a population distribution with statistical ratio in the lower state and no atoms in the upper state. R_{i-3}, the field dependent absorption rate from state i to state 3, is given by

$$R_{i-3} = \frac{g_3}{g_i}\frac{1}{2}AV_i\frac{I_L}{I_s}. \tag{14}$$

These various parameters are

$$\begin{aligned} I_s &= \frac{\hbar\omega_l^3\tilde{\Gamma}}{2\pi c^2}\frac{\pi D}{2\sqrt{\ln 2}\tilde{\Gamma}}, \\ V_i &= \int dx G(x) L(x+\Delta_i^n, \tilde{\Gamma}^n), \\ \tilde{\Gamma}^n &= \frac{2\sqrt{\ln 2}\tilde{\Gamma}}{D}, \\ \Delta_i^n &= 2\sqrt{\ln 2}\frac{\omega_{3i}-\omega_l}{D}, \end{aligned} \tag{15}$$

having introduced the same rate $\tilde{\Gamma}$ for both optical transitions. Here $\hbar\omega_l^3\tilde{\Gamma}/(2\pi c^2)$ is the saturation intensity for a two-level system in the presence of spontaneous emission decay rate for the populations and decay rate $\tilde{\Gamma}$ for the optical coherences. Saturation of the entire Doppler profile increases the saturation intensity to the value I_s by the factor $D/\tilde{\Gamma}$. V_i is the convolution of the normalized Gaussian $G(x)$ and Lorentzian $L(x)$ line shapes.

The steady-state solution for the excited-state population is

$$n_3 = \frac{1}{2}\frac{1}{1+f}, \tag{16}$$

where

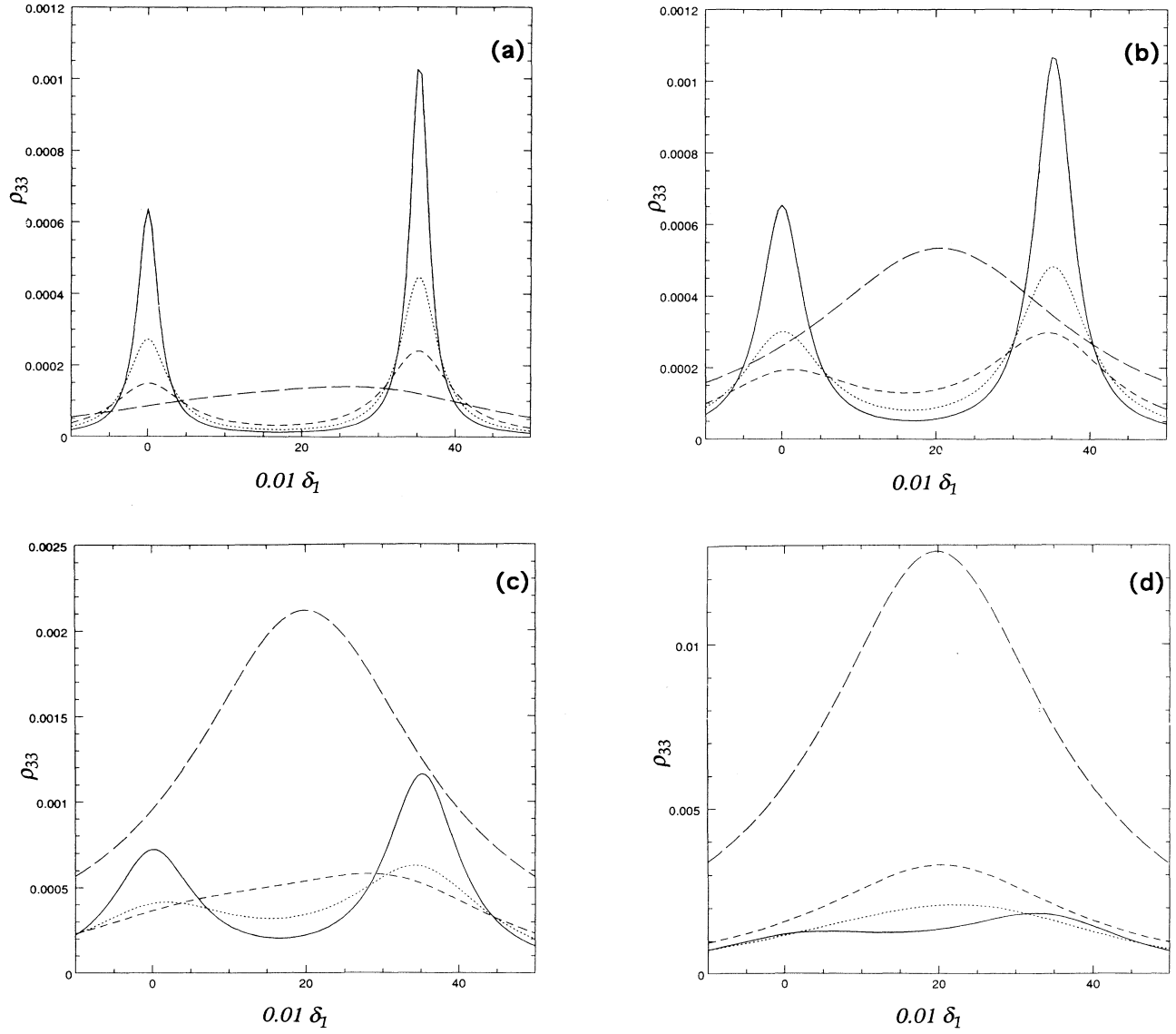

FIG. 8. Dependence of the excited-state occupation ρ_{33} on the laser frequency relative detuning δ_1, as obtained from the numerical analysis of Eq. (4) introducing the cesium transition branching ratios. In (a) $\Omega_1 = \Omega_2 = 5A$, in (b) $\Omega_1 = \Omega_2 = 10A$, in (c) $\Omega_1 = \Omega_2 = 20A$, and in (d) $\Omega_1 = \Omega_2 = 50A$. In each set of curves the bottom continuous line corresponds to $p = 0.2$ Torr, and other curves to 0.5, 1.0, and 5.0 Torr, respectively. The proper value of the γ_t transit rate for each curve is obtained using Eq. (11). Doppler averaging does not significantly modify the results.

$$f = \frac{(b_1 + b_2 - 1)(1+a)\frac{V_1}{2b_1}\frac{V_2}{2b_2}W^2 + \left[b_2\frac{V_1}{2b_1} + b_1\frac{V_2}{2b_2} + \left(\frac{V_1}{2} + \frac{V_2}{2}\right)a\right]W}{2b_1b_2\frac{V_1}{2}\frac{V_2}{2}(1+a)W^2 + \left(\frac{V_1}{2b_1} + \frac{V_2}{2b_2}\right)aW} \tag{17}$$

and

$$a = \gamma_t/A,$$
$$W = \frac{I_L}{I_s(1+a)}. \tag{18}$$

Introducing a saturation intensity $I_s = 250$ mW/cm^2, Eq. (16) reproduces the observed fluorescence intensity line shapes for the laser intensities applied in the experiment. The numerical results obtained from Eq. (16) for the frequency dependence of the fluorescence are reported in Fig. 4 (dotted lines) for comparison with the experimental results. The hyperfine splitting in the excited state has not been explicitly included in the calculation, but it has been taken into account by introducing an effective Doppler broadening $2D/2\pi = 520$ MHz.

V. CONCLUSIONS

In this work we have observed collisional enhanced fluorescence on cesium vapor and we have worked out two models: a density matrix approach that explains the general behavior of the fluorescence, and a simple rate-equation model, that, despite its shortcomings, provides a good quantitative agreement with the observed line shapes, as shown in Fig. 4. The experiment has shown that the interplay of collisional line broadening and saturation leads to dramatic modifications in the fluorescence excitation spectrum. Our model, an improvement with respect to that of Ref. [5], includes the laser saturation and takes into account the relaxation between the ground-state hyperfine levels due to the process of transit through the laser beam. As in the model and experiments on sodium atoms [5], collisions are assumed to be fast, i.e., completely Maxwellizing the atomic velocity distribution. The assumption of a Maxwell-Boltzmann velocity distribution for the atoms in spite of the velocity-selective excitation by the laser, is justified in the regime where the velocity-changing collisions thermalize the velocity distribution rapidly compared to the absorption-emission cycle. The rate of ground-state velocity-changing collisions is proportional to the pressure p of the buffer gas; the absorption rate is proportional to the laser intensity I_L. If, as for sodium atoms, we suppose a cross section of 30 Å^2, the rate for velocity-changing collisions is $(2 \times 10^6\ \text{sec}^{-1}) \times [p\ (\text{Torr})]$. Using the absorption rate $(1 \times 10^7\ \text{sec}^{-1}) \times [I_L\ (\text{mW/cm}^2)]$ for cesium atoms in the laser selected class, we deduce that the Maxwell-Boltzmann velocity distribution will not be modified at all for buffer gas pressure to laser intensity ratios p/I_L larger than 0.2 Torr mW^{-1} cm^2. The sodium experiment of Ref. [5] was performed in conditions of very low laser intensity such that this relation was satisfied. On the contrary the present cesium experiment is performed at laser intensities where this relation is not satisfied. However, in an optical pumping experiment, the final velocity distribution is determined not by a single collision, but by the cumulative effect of a very large number of velocity-changing collisions taking place during the atomic transit time. It has been verified in optical pumping experiments on alkali atoms and other atomic systems, that apart from a small deformation for the velocity class in resonance with the laser, the final distribution is well approximated by a Maxwell-Boltzmann distribution [10]. For instance, for sodium atoms in the presence of low pressure argon buffer gas, with p between 0.2 and 2 Torr, it was shown that at pI_L larger than 50 Torr mW/cm^2, the optical pumping in a dark state was nearly complete for all the velocity classes, with a thermalized velocity distribution. Because the present cesium experiment operates in a range of pressure-intensity values satisfying this last relation, we have used the Mazwell-Boltzmann distribution to describe the atomic velocity occupation. It should also be noticed that the optical pumping in a bright state takes place for the laser frequency not in resonance with an atomic transition, where the deformation of the velocity distribution is smaller. We have performed another test for the velocity distribution by solving a rate-equation model where a slow velocity-changing collision process takes place and we have shown that for the broad structure in the fluorescence spectrum at the center between the two atomic transitions, the two extreme models with total thermalization and very weak velocity-changing process lead to nearly equivalent results. Still, for laser frequencies in resonance with the cesium transitions, differences are expected between the model with total thermalization and the experimental results. If the buffer gas pressure p is low, the hyperfine structure of the excited state may also play an important role and modifies the appearance of the fluorescence spectrum. Indeed the experimental results reported in Fig. 2(b) show that for the curve at the lowest buffer gas pressure, a large deformation of the fluorescence curve is observed around the atomic line, that cannot be described through the total thermalization model.

As a final point, we comment on the laser and atomic parameters required to produce the appearance of the broad central structure in the atomic fluorescence spectrum. From the theoretical analysis and the experimental results, it turns out that the key parameter leading to the broad fluorescence is the ratio between Rabi frequencies Ω_1, and Ω_2 and the relaxation rate of the ground-state populations and coherence, i.e., the transit rate γ_t. That ratio represents the number of optical pumping cycles taking place while an atom interacts with the laser radiation. If the ratio is large compared to 1, the atomic

line shape is heavily distorted and the large central fluorescence is obtained. The Rabi frequencies increase with the laser intensity I_L, while the transit relaxation rate γ_t depends on the laser beam diameter and the buffer gas pressure as given by Eq. (11). For a fixed laser diameter, the ground-state relaxation rate is basically inversely proportional to the buffer gas pressure. Thus the atomic line-shape distortion becomes more important when, all other parameters being constant, the buffer gas pressure or the laser intensity is increased (unless the pressure is high enough that collisions directly relax the population of the ground level).

ACKNOWLEDGMENTS

The authors are grateful to C. Carducci for his contribution in the initial stage of this investigation, to G. Nienhuis for very illuminating discussions on the collision processes and a fruitful reading of the manuscript, to P. Verkerk for testing on his apparatus some cesium optical pumping features, to M. Badalassi for preparing the cesium cells, and to F. Lazzeri for help in setting into operation the laser diodes. This work was partially supported by the Comitato Tecnologico ed Innovazione del CNR and by Consorzio INFM as a part of the project "Heterostructures lasers for atomic physics."

* Also at Max-Planck Institut für Quanten Optik, D-8046 Garching, Germany.

[1] For a review see, for example, *Collisions and Half-Collisions in Laser Fields*, edited by N. Rahman, C. Guidotti, and M. Allegrini (Springer-Verlag, Berlin, 1986).

[2] G. Alzetta, L. Moi, and G. Orriols, Nuovo Cimento B **52**, 209 (1979); G. Orriols, *ibid.* **53**, 1 (1979); I. Siemers, M. Schubert, R. Blatt, W. Neuhauser, and P.E. Toschek, Europhys. Lett. **18**, 139 (1992).

[3] E. Arimondo, in *Interaction of Radiation with Matter, A Volume in Honour of Adriano Gozzini*, edited by G. Alzetta, E. Arimondo, F. Bassani, and L. Radicati (Scuola Normale Superiore, Pisa, 1987), p. 343.

[4] The notation of dark and bright hyperfine ground states as not interacting or interacting with the light has also been introduced in W. Ketterle, K.B. Davis, M. Joffe, A. Martin, and D.E. Pritchard, Phys. Rev. Lett. **70**, 2253 (1993).

[5] R. Walkup, A. Spielfiedel, W.D. Phillips, and D.E. Pritchard, Phys. Rev. A **23**, 1869 (1981).

[6] W.A. Hamel, A.D. Streater, and J.P. Woerdman, Opt. Commun. **63**, 32 (1987); J.E.M. Haverkort, H.G.C. Werij, and J.P. Woerdman, Phys. Rev. A **38**, 4054 (1988).

[7] L. Windholz, T. Neger, and G. Pichler (unpublished).

[8] G. Moe, A.C. Tam, and W. Happer, Phys. Rev. A **14**, 349 (1976); A.C. Tam and G. Moe, *ibid.* **14**, 528 (1976); B. Sayer, M. Ferray, J. Lozingot, and J. Berlande, J. Phys. B **9**, L293 (1976).

[9] W. Happer, Rev. Mod. Phys. **44**, 169 (1972).

[10] P.G. Pappas, R.A. Forber, W.W. Quivers, Jr., R.R. Dasari, M.S. Feld, and D.E. Murnick, Phys. Rev. Lett. **47**, 236 (1981); W.W. Quivers, Jr., R.A. Forber, A.P. Ghosh, D.J. Heinzen, G. Shimkaveg, M.A. Attili, C. Stubbins, P.G. Pappas, R.R. Dasari, M.S. Feld, Y. Niv, and D.E. Murnick, in *Laser Spectroscopy V*, edited by A.R.W. McKellar, T. Oka, and B.P. Stoicheff (Springer-Verlag, Berlin, 1981), p. 186.

[11] K.E. Gibble and A. Gallagher, Phys. Rev. A **43**, 1366 (1991).

[12] D. Tupa, L.W. Anderson, D.L. Huber, and J.E. Lawler, Phys. Rev. A **33**, 1045 (1986).

[13] C. Wieman and L. Hollberg, Rev. Sci. Instrum. **62**, 1 (1991).

[14] R. Brewer and E.L. Hahn, Phys. Rev. A **11**, 1641 (1975); G. Orriols, Nuovo Cimento B **53**, 1 (1979).

[15] R.O. Garrett, S.Y. Ch'en, and E.C. Looi, Phys. Rev. **156**, 48 (1967); N. Allard and J. Kielkopf, Rev. Mod. Phys. **54**, 1103 (1982).